

# Neutron production and thermal moderation at the PSI UCN source

H. Becker<sup>a,b</sup>, G. Bison<sup>a</sup>, B. Blau<sup>a</sup>, Z. Chowdhuri<sup>a</sup>, J. Eikenberg<sup>a</sup>, M. Fertl<sup>a</sup>,  
K. Kirch<sup>a,b</sup>, B. Lauss<sup>a,\*</sup>, G. Perret<sup>a</sup>, D. Reggiani<sup>a</sup>, D. Ries<sup>a</sup>,  
P. Schmidt-Wellenburg<sup>a</sup>, V. Talanov<sup>a,\*\*</sup>, M. Wohlmuther<sup>a</sup>, G. Zsigmond<sup>a</sup>

<sup>a</sup>*Paul Scherrer Institute, CH-5235 Villigen PSI, Switzerland*

<sup>b</sup>*Institute for Particle Physics, Eidgenössische Technische Hochschule, Zürich,  
Switzerland*

---

## Abstract

We report on gold foil activation measurements performed along a vertical channel along the tank of the ultracold neutron source at the Paul Scherrer Institute. The activities obtained at various distances from the spallation target are in very good agreement with MCNPX simulations which take into account the detailed description of the source as built.

*Keywords:* neutron transport simulation, thermal neutron, neutron activation, neutron flux, spallation target, ultracold neutron source

*PACS:* 28.20.Gd, 28.20.-v, 29.25.Dz, 61.80.Hg

---

## 1. Introduction

Since 2011, the high-intensity ultracold neutron (UCN) source [1, 2, 3, 4] is being operated at the Paul Scherrer Institute (PSI), Villigen, Switzerland. The UCN facility serves mainly fundamental neutron physics experiments. Ultracold neutrons have energies below about 300 neV, corresponding to milli-Kelvin temperatures. UCN can be stored in vessels where they can be observed for hundreds of seconds [5].

The first experiment installed at the new facility is an improved search for the neutron electric dipole moment (nEDM) [6]. The search for the

---

\*Corresponding author, bernhard.lauss@psi.ch

\*\*Corresponding author, vadim.talanov@psi.ch

nEDM is considered to be one of the most important experiments in particle physics today (see e.g. [7, 8, 9]) and will contribute to solving the puzzle of the matter-antimatter asymmetry observed in our universe. The present best nEDM limit [10] can only be improved with a higher experimental sensitivity and needs a higher intensity of ultracold neutrons.

The PSI UCN source uses solid deuterium to produce UCN. The intensity of UCN provided to the experiments is proportional to the thermal neutron flux entering the solid deuterium moderator. The understanding of the neutron flux from the spallation target, its thermal moderation and its spacial and energetic variation over the UCN source volume is essential for assuring the highest possible thermal neutron production and maximal UCN production. A comparable spallation-based UCN source has been operated at the Los Alamos National Laboratories for several years [11, 12].

In this paper we compare results from measurements of the neutron flux using gold foil activation and simulation of these measurements using MC-NPX [13].

The outline of the paper is as follows: First we give a short introduction to the UCN source (Sec. 2). We describe the neutron production simulation and the spallation target (Sec. 3). In Sec. 4. the gold foil activation measurements are discussed. Next, the Monte Carlo simulation of the neutron flux using the numerical model of the UCN source is explained (Sec. 5). The results section 6 compares calculated activities and measurements which are then discussed and summarized in Sec. 7.

## 2. The ultracold neutron source

The operating principle and progress of the PSI UCN source have been documented in [1, 2, 3, 4]. A sketch of the UCN tank displaying the parts relevant for the investigations presented here is given in Fig. 1.

The neutron production is based on proton induced spallation of lead. The 590 MeV protons from the PSI cyclotron [14, 15] are available at 2.2 mA beam current 24 hours per day. The UCN source operates at about 1% duty cycle with up to 8 s long proton beam pulses at full beam current impinging on the target, corresponding to 20  $\mu$ A average beam current. A typical operation with 4 s beam pulses allows a beam pulse repetition time of 440 s.

The resulting neutron flux off the spallation target of about  $10^{17}$  neutrons/s (the neutron yield is about 7 – 8 n/p [16]) during the beam kick is thermalized by heavy water ( $D_2O$ ) surrounding the target at an operating

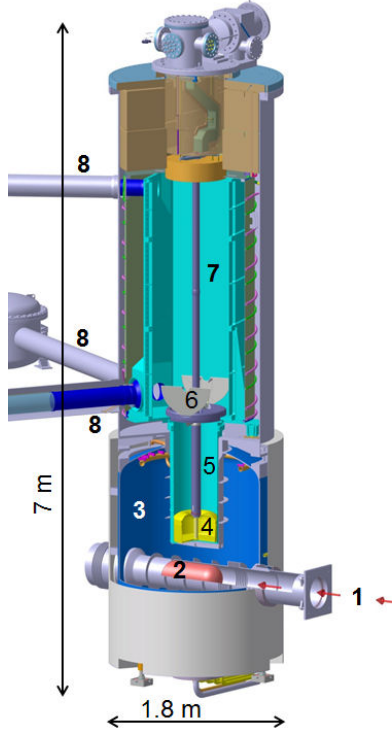


Figure 1: Sketch of the UCN tank with parts important to this work: (1) Proton beam channel from cyclotron, (2) spallation target, (3) heavy water moderator tank, (4) deuterium moderator vessel, (5) vertical UCN guide, (6) UCN storage vessel shutter, (7) UCN storage vessel, (8) UCN guides to experiments.

temperature of  $31^{\circ}\text{C}$ . Subsequently, about 30 liters of solid deuterium inside the  $\text{D}_2$  moderator vessel at a temperature of about 5 K are used as cold moderator and superthermal UCN converter [17]. After the beam pulse the UCN are trapped in the UCN storage vessel with its bottom shutter closed. About 8 m long UCN guides which penetrate the biological shielding provide UCN to experiments in two different experimental areas; the nEDM experiment is located in area South.

### 3. Neutron production and moderation

#### 3.1. Spallation target

After acquiring the final beam energy of 590 MeV in the PSI ring cyclotron the full proton beam is deflected using a kicker magnet [18] towards the UCN spallation target. Before impinging on the target, monitors check the proton beam's center and profile. The profile of the proton beam at the target, as derived from the beam optics calculation, follows a two dimensional Gaussian distribution with  $\sigma_{x,y} = 4$  cm, cut by collimators at a radius of  $r=10$  cm from the beam axis [19]. The corresponding intensity of the beam on target is 95% of the nominal 2.2 mA current for the measurements regarded in this paper.

Before the system had been built studies of neutron yield, moderation, UCN production and radiation environment [20] lead to an initial UCN source design. A comprehensive study of a more detailed geometry of spallation target and target region followed optimizing the target mechanical design with respect to neutron production and thermo-mechanical behavior [16].

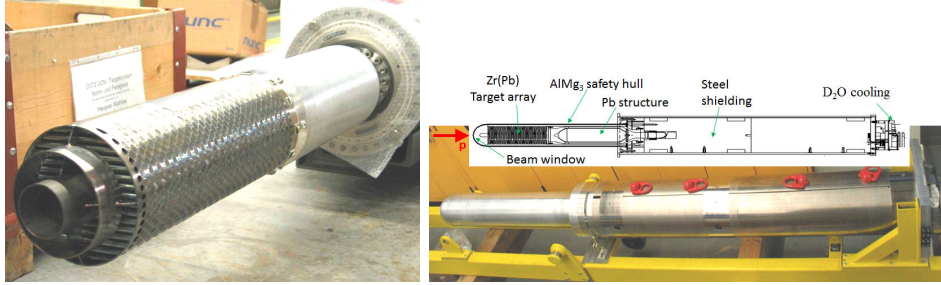


Figure 2: Top: Photo of the “Cannelloni” array of the spallation target, consisting of lead-filled Zircaloy tubes. Two cylindrical flow guides made from 2 mm thin aluminum direct the D<sub>2</sub>O coolant flow in front of the target.

Bottom: Photo and cut view of the assembled target with safety hull ready for installation. The total length of the target assembly is 390 cm, the total weight about 2000 kg.

The UCN source now utilizes the “Cannelloni” type spallation target assembly which has been developed and successfully used for a decade at PSI at the Swiss spallation neutron source SINQ [21]. Fig. 2 shows a photo of the spallation target before its installation at the UCN source. The target array, with a length of 55 cm and a radius of 10.5 cm consists of 760 Zircaloy tubes with 10.75 mm outside and 9.25 mm inside diameter, each filled with lead at a filling factor of 90%. The total mass in the target is 93 kg of lead, 21 kg of Zircaloy and 7.5 kg of D<sub>2</sub>O. The target array is contained in

an AlMg3 safety hull together with necessary shielding and cooling tubes, as shown in Fig. 2. The cooling agent is heavy water at a mass flow rate of 22 kg/s. The minimal proton beam path length in D<sub>2</sub>O from the target hull to the front Zircaloy tube is 14 cm. The target assembly is inserted into a vacuum tube penetrating the heavy water tank. This tank has an inside diameter of 160 cm and a height of 180 cm and contains 3300 liter of D<sub>2</sub>O at room temperature serving as thermal moderator for the primary neutron flux.

### 3.2. Calculation of the primary neutron yield

A full simulation of the neutron production and moderation in the UCN source setup was conducted in order to establish a consistent description of the activity measurements. The neutron flux density distribution starting from the proton beam impact on the spallation target was calculated using the Monte Carlo radiation transport code MCNPX version 2.7.0 [13] with standard  $S(\alpha, \beta)$  tables. The MCNPX geometry description followed in detail the “as-built” construction of the UCN source, including a realistic simulation model of the spallation target array, cooling arrangement and target container [16]. In the present study the primary neutron yield from the target was simulated as illustrated in Fig. 3. The neutron yield is calculated by surrounding the geometric representation of the physical target, the target cell, by a target envelope. The source of primary protons was placed inside this MCNPX target cell, but outside the target entrance sphere. Neutrons produced by nuclear reactions inside the target cell which leave the target cell will cross the target envelope and directly contribute to the outgoing flux  $N_{out}$  (green trajectories in Fig. 3). However, neutrons produced in the target which left the target cell and returned after being scattered in the surrounding structures will be monitored and contribute to the incoming flux  $N_{in}$  and tagged incoming flux  $N'_{in}$  (yellow arrow) to avoid double counting of neutrons. If such neutrons once again leave the target cell, they will be monitored as well and contribute to the tagged outgoing flux ( $N'_{out}$ , red arrow).

This model allows us to calculate the primary neutron yield from the target  $N_0 = N_{out} - N'_{out}$ .  $N_0$  is the number of neutrons produced in the target cell by the incident proton beam and subsequent particle cascade(s), excluding those produced by secondary particles (or by their products) that passed the target envelope but then were scattered back and passed the target cell once again.

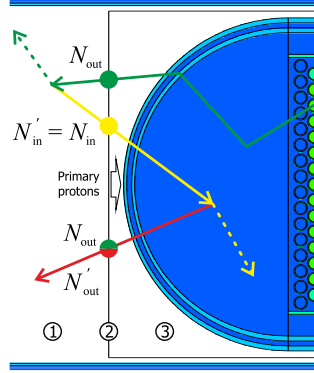


Figure 3: Sketch of parts of the MCNPX spallation target geometry model showing possible neutron trajectories following primary neutron production by beam protons modeled within MCNPX. (1) Tagging region, (2) MCNPX target envelope, (3) MCNPX target cell. The cylindrical flow guides are not shown and irrelevant for the simulation.

Another way to calculate this quantity is to compute it from the data available in the MCNPX output summary tables, that can be a computationally tedious and strictly geometry-dependent procedure (as in [16]). In contrast, the method used here depends only on few surfaces that define the target envelope and the cells that are used for tagging.

The result of our calculation is a neutron yield of 7.27 neutrons per primary proton at the target [22] which is in good agreement with the previous estimate of 7.62 neutrons per primary proton at the target from [16], within the 5% estimated error of the calculations.

This value can be compared to the measured neutron yields for the 61 cm long Pb targets as reported in [23], which are given in Tab. 1 after interpolation to the incident proton beam energy of 590 MeV. The comparison shows that the design of the spallation target of the UCN source provides effective neutronic performance, ensuring at the same time the optimal thermo-mechanical behavior required for the high intensity beam conditions.

Due to the D<sub>2</sub>O cooling of the spallation target, neutrons can already be thermalized inside the target safety hull and either be captured or leave the target cover pre-moderated. Fig. 4 compares the energy spectra of neutrons at the point of leaving the target envelope for the case simulated with and without D<sub>2</sub>O inside the target envelope. Neutron energies down to the thermal (meV) region demonstrate the moderation effect already inside the target envelope.

target	neutron yield per proton	Pb mass ( <i>kg</i> )	neutron yield per proton per lead atom
solid, $\varnothing=10.2$ cm	9.78	57	$5.9 \times 10^{-26}$
solid, $\varnothing=20.4$ cm	11.2	226	$1.7 \times 10^{-26}$
filled “Cannelloni”	7.27	93	$2.7 \times 10^{-26}$

Table 1: The result of our calculation for the primary neutron yield per incident beam proton from the filled “Cannelloni” spallation target of the UCN source compared to the measured neutron yields from solid 61 cm long Pb targets with diameters  $\varnothing$  as reported in [23] interpolated to the PSI proton beam energy.

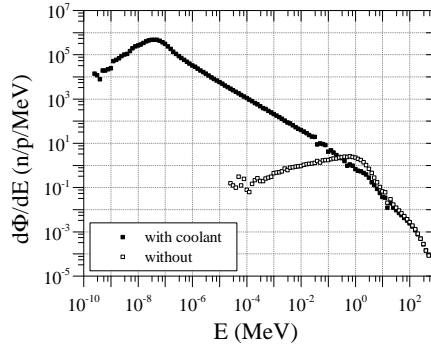


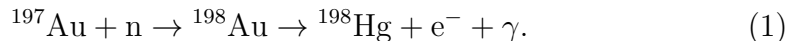
Figure 4: Calculated energy spectrum of the neutrons, given in neutrons per proton per MeV, at the point of leaving the “target envelope” of Fig.3 for the cases with (filled squares) and without (empty squares) D<sub>2</sub>O coolant inside the target envelope.

#### 4. Gold foil activation measurements

The number of produced UCN is directly proportional to the number of spallation neutrons and the number of thermal neutrons entering the solid deuterium converter [17]. Many restrictions, most notably the very high radiation environment, prevent access to the solid deuterium moderator vessel. However, the thermal neutron flux can be measured in a distance of about 1 m from this region of interest, outside the UCN vacuum and heavy water tank. These measurements can directly be compared with the numerically estimated neutronic performance of the target-moderator system and thus serve to indirectly check the neutron flux delivered to the solid deuterium moderator, which can be predicted by the simulations as well.

#### 4.1. Measurement principle

The measurement technique is based on the neutron activation of gold foils,



The  $\beta$ -decay half-life of  $^{198}\text{Au}$  is 2.6947(3) days with well known  $^{198}\text{Hg}$   $\gamma$  intensities and energies of 411.8 keV for the main transition, and 675.9 keV 1087.7 keV [24]. The initial gold activity is calculated from the measured absolute  $\gamma$  intensity. This activity can then be compared to the one derived from a full simulation which takes into account the proton beam energy and shape, neutron production via spallation, neutron moderation, neutron transport through the system and activation of the  $^{197}\text{Au}$  via neutron capture for the neutron flux and energy spectrum at the measurement position.

#### 4.2. Setup for the gold-foil irradiation

The experimental setup uses gold foils deployed on a nylon rope along the UCN tank. The drawing of the tank in Fig. 5 shows the position of the aluminum tube which contains the rope. Nylon was used to minimize activation of the rope material. The 16 mm inside diameter tube horizontally penetrates about 3 m of the biological shielding of the UCN source and then turns down along the outside of the tank to the floor with a reduced inner diameter of 12 mm. There the sharp bend and a welding connection pose the tightest constraints for the insertion of any device. This tube is the best access port to measure the thermal neutron flux. It is closed during regular operation.

The length of the insertion tube was measured with a steel rope pushed down the tube and then extracted again. The tube length of  $10.70 \pm 0.01$  m is in agreement with the design drawing of  $10.72 \pm 0.02$  m. Pushing the steel rope one could feel a resistance after 4.75 m into the tube which was identified as welding joint, where the inner diameter is reduced to estimated 8.5 mm. A similar measurement was done using a nylon rope which was compressed and slightly curled inside the tube. Two measurements yielded  $10.82 \pm 0.01$  m which define a correction factor of  $0.989 \pm 0.002$  to the nylon rope length. To account for eventual changes of compression or twisting when the rope with the foils was finally inserted, e.g. due to friction or roughness changes, a conservative estimate of the position error of 5 cm was used in the analysis. Although the errors on the position of the foils will not be independent



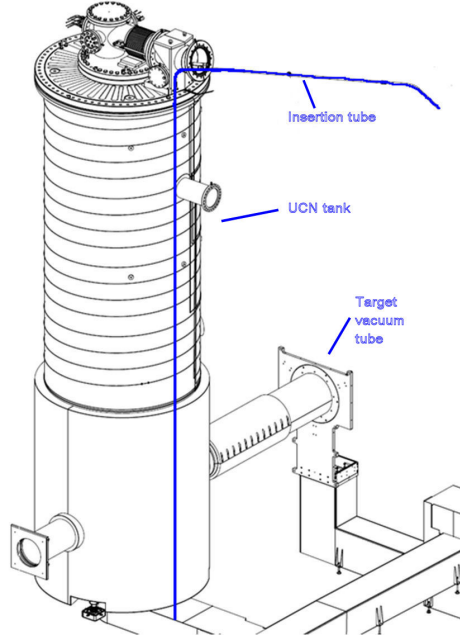


Figure 5: Drawing of the 7 m high UCN tank. The vacuum tube for the spallation target penetrates the D<sub>2</sub>O tank which reaches 143 cm above the center of the target. The Al "insertion tube" along the tank is indicated.

because of the rope, we can neglect this, as a better position resolution is not relevant in this study.

The foils used were 99.95% purity gold ( $^{197}\text{Au}$ ) with a thickness of  $25\text{ }\mu\text{m}$  from Goodfellow, laser-cut into discs with 25 mm diameter. After cleaning with isopropyl alcohol, the foils were weighed three times with a laboratory balance 770-12 by Kern und Sohn. The averaged results are listed in tables 2 and 3 with a 1 mg error on the calibration of the balance. Finally, the foils were attached to the rope using heat-shrink tubing and aluminum foils as shown in Fig. 6.

Three measurement assemblies were used, one for the test measurement, one for the height profile, and one with a cadmium shielded foil. The thicknesses of the used materials were: rope = 6.7 mm, aluminum foil = 0.01 mm, heat-shrink tubing = 0.4 mm. In the setup with the additional 0.55 mm thick Cd covers the rope thickness was reduced to 2.2 mm. The Cd covered foil was positioned in the center of two uncovered gold foils 19 cm apart. The intended position of the gold foils were accurately marked on the rope before

assembly in order to guarantee the position. The foil positions are listed in tables 2 and 3.

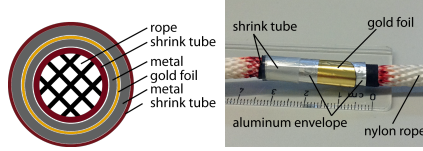


Figure 6: a) Sketch of the mounting assembly for the gold foils on the nylon rope. After a layer of heat-shrink tubing the aluminum-foil-covered gold foil was wrapped around the rope. Then another shrink tube held the sandwich in place. In the measurement with Cd the additional foil covered both sides of the gold. The heat-shrink tubing was used to secure the foils in place.

b) Photo of the rope during probe assembly with part of the Al foil on the outside removed.

#### 4.3. Irradiation of the samples at the UCN source

The following irradiations were conducted using three setups:

1. Preparatory measurement with a single gold foil positioned at beam height to test the feasibility of the foil insertion and irradiation. 2012-10-18: proton pulse length =  $(57 \pm 4)$  ms; beam current =  $(2186 \pm 44)$  mA.
2. A neutron-energy-sensitive measurement with two gold foils and one additional Cd covered gold foil. 2012-11-14: proton pulse length =  $(507 \pm 4)$  ms; beam current =  $(2195 \pm 44)$  mA.
3. A height profile measurement along the UCN tank with 16 gold foils positioned from about 1 m below to 5 m above the beam plane. 2012-11-21: proton pulse length =  $(2007 \pm 4)$  ms; beam current =  $(2197 \pm 44)$  mA.

The error on the proton beam current is estimated to be about 2 % resulting from the absolute calibration error of the proton beam current monitor (MHC1), installed on the proton beam line after the exit of the cyclotron. The given beam pulse length reflects the sum of the pilot and main beam pulse. The maximum error on the irradiation time of  $\pm 4$  ms is estimated from the 1 ms rise-and-fall time of the beam kicker power supply [18] adding up pilot and main pulse transients.

#### 4.4. Determination of the gold activation via $\gamma$ -ray analysis

The  $\gamma$ -ray analysis following the activation was performed at the radioanalytical laboratory of PSI which is an official Swiss accredited laboratory for the survey and analysis of radioisotopes for emission and incorporation. In our measurements we employed an efficiency calibrated high purity N-type Ge detector from ORTEC with 101 cm<sup>3</sup> active volume to determine the  $\gamma$  intensity.

The 25 mm diameter gold foil shape was selected to match the requirements for the geometry setup previously calibrated to  $\pm 5\%$  detection efficiency. The gold foil was pressed to lie flat on the measurement position before the measurement. Measurements lasted between 10 min and 40 min, depending on the sample activity. In Fig. 7 we show the measured  $\gamma$  energy spectrum for foil 4. The dominant line at 411.8 keV is from the  $^{198}\text{Hg}$   $2^+ \rightarrow 0^+$  transition. The electronic K transition X rays in Hg are visible at 70 and 80 keV.

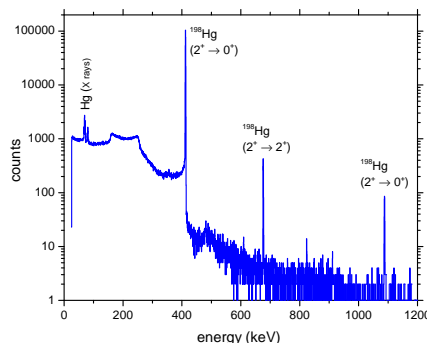


Figure 7: Energy spectrum of  $\gamma$ -rays observed for foil 4 after 20 minutes of measurement time.

The spectroscopy program InterWinner 5.0 by ORTEC was used for the energy spectrum analysis. The measured intensity is corrected for the time period between  $\gamma$  measurement and irradiation, recorded with 1 s accuracy, DAQ dead time and energy dependent detector efficiency. The measured environmental background on the  $10^{-4}$  Hz/channel level is automatically subtracted but negligible here. The background under the relevant  $\gamma$  peak is due to Compton scattering of higher-energy  $\gamma$  rays and automatically subtracted by the software. The results of our analysis for the measured activities of the

foils and their positions are summarized in tables 2 and 3. The  $\pm 5\%$  error on the absolute efficiency calibration of the  $\gamma$  detector is included in the final error. A comparison with the simulation can be done after normalization with irradiation time (beam pulse length) and proton beam current.

The results of Tab. 2 and 3 plotted in Fig. 13 show that the activity maximum corresponds to the beam plane position. The drop in activity at about 1.4 m, corresponds to the top of the heavy water tank.

measurement	position ( <i>cm</i> )	foil mass ( <i>mg</i> )	specific activity ( <i>kBq/g</i> )
preparatory	0.0	$174.9 \pm 1.0$	$1378. \pm 122.$
Au-down	107.9	$262.5 \pm 1.0$	$169.5 \pm 9.3$
Au-Cd-center	117.4	$261.4 \pm 1.0$	$22.8 \pm 1.2$
Au-up	126.9	$251.9 \pm 1.0$	$135.0 \pm 7.3$

Table 2: Results of the preparatory measurement (single foil) and the measurement with the Cd-covered foil vertically centered between two gold foils 19 cm apart. The position is given as vertical distance to the proton beam plane = 0, + is in upward direction. The absolute position uncertainty for every measurement point is estimated to be  $\pm 5$  cm, but this uncertainty is not relevant for this measurement. The measured specific activity is given by the measured  $\gamma$  activity corrected for time period between irradiation and measurement, decay branching, DAQ dead time and detector efficiency, normalized to an irradiation time of 1 s at a proton beam current of 2.2 mA. The given uncertainty includes the  $\pm 5\%$  calibration error on the absolute efficiency of the  $\gamma$  detector.

## 5. Numerical simulation of the thermal neutron flux

In the present simulation we have used a description with — in comparison to the early design [20] — many more construction details of the UCN tank and the area surrounding the target, such as the support structure of the heavy water moderator tank, the outer shell of the UCN source, UCN storage vessel etc. [25]. A vertical cut of the MCNPX geometry model with definitions used in the particle transport simulation is shown in Fig. 9, some important dimensions are given in Tab. 4. A photo of the heavy water (bottom) part of the UCN tank during construction displaying some details of the surroundings is shown in Fig. 8.

After simulation of the initial neutron production, as described in Sec. 3.2, MCNPX was used to further track the neutrons. The neutron flux density

foil number	position ( <i>cm</i> )	foil mass ( <i>mg</i> )	specific activity ( <i>kBq/g</i> )
1	-73.3	$233.4 \pm 1.0$	$388. \pm 21.$
2	-48.6	$232.2 \pm 1.0$	$753. \pm 41.$
3	-23.9	$241.0 \pm 1.0$	$1198. \pm 65.$
4	0.9	$237.0 \pm 1.0$	$1333. \pm 72.$
5	25.6	$242.9 \pm 1.0$	$1040. \pm 56.$
6	50.3	$227.7 \pm 1.0$	$654. \pm 35.$
7	75.0	$242.3 \pm 1.0$	$359. \pm 19.$
8	99.8	$230.0 \pm 1.0$	$191. \pm 10.$
9	124.5	$237.0 \pm 1.0$	$147. \pm 8.$
10	149.2	$245.0 \pm 1.0$	$68.2 \pm 3.7$
11	173.9	$242.1 \pm 1.0$	$50.7 \pm 2.7$
12	198.6	$211.0 \pm 1.0$	$45.0 \pm 2.5$
13	248.1	$224.8 \pm 1.0$	$35.3 \pm 1.9$
14	297.5	$226.6 \pm 1.0$	$26.3 \pm 1.4$
15	396.4	$234.4 \pm 1.0$	$14.5 \pm 0.8$
16	495.3	$241.6 \pm 1.0$	$1.45 \pm 0.10$

Table 3: Results of the height profile measurement. Positions and uncertainties as described in the caption of Tab. 2.

was simulated in the gap between the outer wall of the UCN tank and the innermost shielding blocks of the UCN source (see Fig. 10). Fig. 11 shows the distribution in the horizontal proton beam plane defined through the horizontal axis of the spallation target perpendicular to the plane of Fig. 9. A neutron energy of 0.5 eV was used as lower threshold definition for the epithermal flux component. The numerical activity results with and without Cd shielding however used the full neutron energy information.

The numerical values of the total and epithermal neutron flux density from Fig. 11 for four angles in the proton beam plane are given in Tab. 5. The neutron flux density in the beam plane has a clear maximum towards the incoming proton beam ( $\phi = 90^\circ$ ) due to the small amount of material in this region. The ratio of epithermal to total neutron flux density at this angle is  $\sim 1/3$  larger than at  $\phi = 0^\circ$  or  $180^\circ$ . The dip in the total neutron flux density at  $\phi = 270^\circ$  corresponds to the position of the lead shielding cylinder

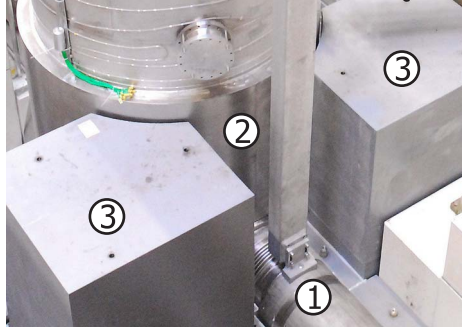


Figure 8: Photo of the bottom part of the UCN tank during construction of the UCN source: (1) Outer vacuum vessel for the spallation target, (2) D<sub>2</sub>O tank surrounded by (3) iron shielding.

	part	material	thickness ( <i>cm</i> )
a)	wall of the UCN tank (bottom)	Al	0.3
b)	wall of the UCN tank (top)	steel	1.0
c)	bottom and top ring of the D <sub>2</sub> O tank	Al	20
d)	top lid of the D <sub>2</sub> O tank	steel	3.0
e)	wall of the UCN storage vessel	Al	0.3
f)	vertical UCN guide wall	Al	0.3
g)	vertical UCN guide bottom	Al	0.3
h)	wall of the D <sub>2</sub> O tank	Al	1.2
i)	wall of proton beam tube	Al	0.25

Table 4: List of material thicknesses of important structural parts (see Fig. 9) of the MCNPX geometry model.

that is located inside the target downstream of the Zr-Pb array. There half of the escaping neutrons possess energies above 0.5 eV. Both, the total and the epithermal flux densities at  $\phi = 0^\circ$  are equal to the respective values at  $180^\circ$  within the statistical error of the simulation, as the MCNPX model above the spallation target is axially symmetric. The fraction of epithermal neutrons at the position of the insertion tube (Fig. 11 dashed line) was calculated to be about 14%. The variation of both total and epithermal neutron flux densities over the azimuthal angle is found insignificant in this position. The estimated angular uncertainty of  $\sim 1.5^\circ$  on the verticality of the insertion-tube positioning has a negligible effect on the results of the simulation.

In the MCNPX model 118 identical gold-foil units were positioned inside

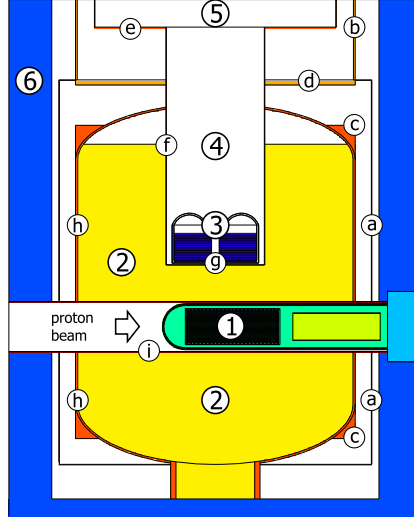


Figure 9: Drawing of the MCNPX geometry model of the central part of the UCN source: (1) “Cannelloni” spallation target (Zr,Pb) with the forward neutron lead shielding (right side), (2) D<sub>2</sub>O tank (Al), (3) solid deuterium vessel (AlMg3, AlMg4.5, Al), (4) vertical UCN guide (Al), (5) UCN storage vessel and shutter (Al), (6) innermost shielding, and structural details of the UCN source a) — i) (see Table 4).

the insertion tube in 5 cm steps from  $-92.5$  cm below to  $+497.5$  cm above the beam plane. The geometry model of each gold foil unit followed the experimental setup described in Sec. 4. The neutron flux density and energy spectra were simulated in the exact MCNPX volume of the gold foil of each gold foil unit.

The material budget and the implemented geometry details in the full MCNPX geometry model shown in Fig. 9 contain many details of the setup, but could in principle still be further improved in terms of minute details. To evaluate the impact of geometrical uncertainties on the numerical results, the MCNPX simulation was run with a reduced geometry model of the UCN source, in which the structural details (a) — (d) from Fig. 9 were removed. Neutron flux density distributions simulated with full and reduced MCNPX geometry representation are compared in Fig. 12. The statistical error of the simulation at beam height (0 cm) is below  $\pm 2\%$  for both total and epithermal neutron flux.

An increase of the epithermal neutron flux by  $\sim 10\%$  is observed in the simulation with the reduced MCNPX model between  $-50$  and  $+100$  cm height. At the same time practically no difference in total neutron flux is

$\Phi \searrow$ angles	$0^\circ$	$90^\circ$	$180^\circ$	$270^\circ$
$\Phi_{tot}$	2.20	7.18	2.21	2.83
$\Phi_{epi}$	0.37	1.85	0.38	1.23
$\Phi_{epi}/\Phi_{tot}$	0.17	0.26	0.17	0.44

Table 5: Total,  $\Phi_{tot}$ , and epithermal,  $\Phi_{epi}$ , neutron flux density per incident proton on the target ( $10^{-4}$  n/cm<sup>2</sup>/p) and epithermal fraction at different angles in the proton beam plane.

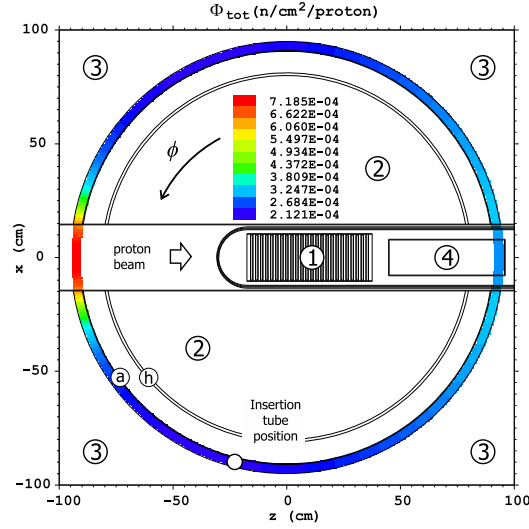


Figure 10: Total neutron flux density distribution  $\Phi_{tot}$ (n/cm<sup>2</sup>/p) simulated around the UCN tank in the beam plane versus azimuthal angle  $\phi$ : (1) “Cannelloni” spallation target (Zr,Pb) with the (4) forward lead shielding, (2) UCN tank, (3) innermost shielding (structural details a) and h) defined in Table 4)).

found in this region. Above 150 cm, the two estimates differ by more than a factor of two, indicating that in the top region more detailed modeling would be required.

A separate simulation study changing the operating temperature and hence the density of the heavy water moderator from 31°C by  $\pm 10^\circ\text{C}$  showed a negligible change of the neutron flux.

## 6. Calculation of activities and comparison to measurement results

The neutron flux density and energy spectra simulated as described in Sec. 5 were used to calculate the induced  $^{198}\text{Au}$  activity in the gold foils using



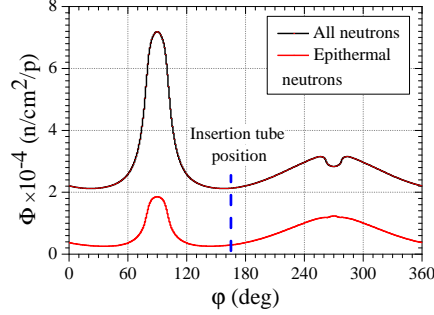


Figure 11: Simulated neutron flux density distribution  $\Phi$  per incident proton on the target around the UCN tank in the beam plane as a function of the azimuthal angle, for all and for epithermal neutron energies. Position  $\phi = 0$  is perpendicular to the direction of the proton beam. The position of the insertion tube for the Au foils at about  $165^\circ$  is indicated.  $90^\circ$  is opposite to the proton beam direction.

the build-up and decay code FISPACT07 [26]. An automated procedure of activity calculation using the results of the MCNPX simulation was provided by the Activation Script [27]. The result of the calculation, the position dependent specific  $^{198}\text{Au}$  activity of the gold foils along the UCN tank, is given in Tab. 6.

In Fig. 13 the results of the activity calculation for the simulated neutron flux using the full and the reduced MCNPX geometry model are compared to the activity measurements provided in Tab. 2 and 3. The statistical error of the activity calculations between  $-100$  and  $+150$  cm is below  $\pm 4\%$  for both geometry models. Above  $150$  cm the statistical error is  $\sim 20\%$  for the full model and  $\sim 10\%$  for the calculation with the reduced MCNPX model. This precision is completely sufficient for our purposes.

An additional MCNPX calculation was done in the full model in order to compare to the measurement with the cadmium (Cd) covered foil at  $y=117$  cm which is only sensitive to the epithermal neutron flux. The results for the Cd covered gold foil are compared with the corresponding adjacent uncovered gold foils in Tab. 7 and are also shown in Fig. 13. The epithermal neutron contribution to the unshielded gold activity at the measurement position is only around  $15\%$ . Therefore, even a large error on the knowledge of the epithermal neutron flux contributes relatively little to the error of the activity from the total neutron flux.

The crucial quantity of interest for the production of ultracold neutrons

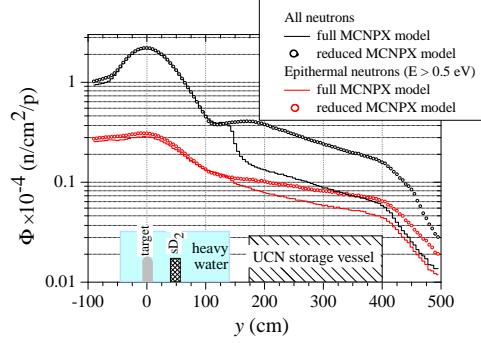


Figure 12: Simulated neutron flux density distribution at the position of the insertion tube  $\Phi$  per incident proton on the target versus height ( $y$ ) along the UCN tank at the position of the insertion tube, for all and for epithermal neutron energies. Results are compared for the simulations with the full MCNPX model (solid lines), and the reduced MCNPX model (open symbols). Major parts inside the UCN tank are indicated at their approximate  $y$ -position.

is the thermal neutron flux entering the solid deuterium moderator vessel located about 50 cm above the proton beam plane. As the thermal neutron flux at this specific position cannot be directly probed, one has to compare experiment and simulation results at accessible positions. The measured  $^{198}\text{Au}$  activity at this height is  $654 \pm 35$  kBq/g. It has to be compared with the values calculated with the full,  $626 \pm 16$  kBq/g, and the reduced,  $688 \pm 8$  kBq/g, MCNPX model. The two models differ only by about 10% at this position. The very good agreement between measured and calculated activities demonstrates that the combination of neutron production in the Cannelloni target and subsequent moderation in the surrounding  $\text{D}_2\text{O}$  are accurately modeled by MCNPX and understood.

## 7. Summary and discussion

The measurements of the gold activity along the UCN tank from 1 m below to  $\sim 3$  m above the proton beam plane are well matched by the full MCNPX model (see Tab. 6). A correct simulation of the thermal neutron flux along the height is only possible with a realistic description of structural details inside and the presence of shielding outside of the tank. For our “full” model the result of the simulation differs to measurements up to 50% if one looks at heights of 4 m above beam plane. A more detailed modeling would

position (cm)	$A_{sp}$ (kBq/g)	$D_{MS}$
-73.3	438.	-0.12
-48.6	599.	0.23
-23.9	944.	0.24
0.9	1090.	0.20
25.6	930.	0.11
50.3	626.	0.04
75.0	378.	-0.05
99.8	215.	-0.12
124.5	187.	-0.24
149.2	98.	-0.35
173.9	59.	-0.15
198.6	49.	-0.09
248.1	44.	-0.21
297.5	29.	-0.12
396.4	23.	-0.48
495.3	3.8	-0.90

Table 6: Results for the height dependent activity simulation. The position of the gold foil is given as in Tab. 3. Simulated specific activities  $A_{sp}$  are normalized to an irradiation time of 1s at 2.2mA proton beam current. Column 3 gives the relative difference between simulation and measurement (Tab. 3)  $D_{MS} = (A_{sp}(\text{measurement}) - A_{sp}(\text{simulation})) / (A_{sp}(\text{measurement}) + A_{sp}(\text{simulation})/2.)$

be required for the top region to reach better matching but was discarded, as this is not required to understand the UCN production.

An assessment of the epithermal neutron flux at 117cm above the beam plane was done with a comparison measurement of a cadmium covered gold foil. The measurement shows a 15% fraction of epithermal neutrons at that position, while the simulation gives a  $\sim 10\%$  fraction. This difference contributes relatively little to the total activity value and the determination of the thermal flux.

The primary region of interest for the production of ultracold neutrons is the location of the solid deuterium moderator vessel. The  $^{198}\text{Au}$  activity measurement at this beam height of about 50cm falls between the values calculated with the full and the reduced MCNPX model, the two models

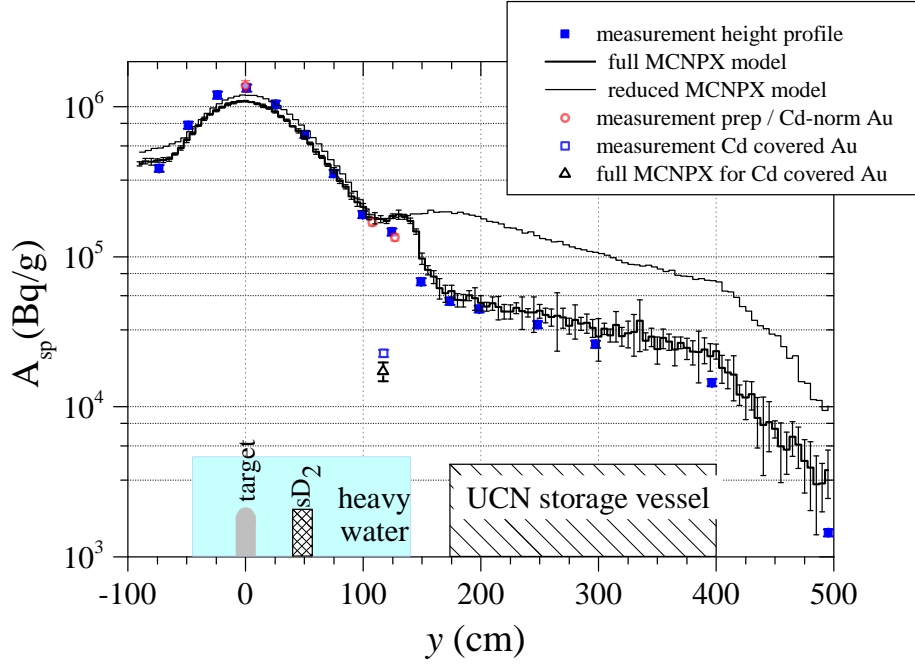


Figure 13:  $^{198}\text{Au}$  specific activity  $A_{sp}$  (Bq/g) versus height ( $y$ ) along the UCN tank after irradiation with a 1 s long beam pulse at 2.2 mA proton beam current. Comparison of simulations with the full MCNPX model (bold solid line) with statistical errors, and the reduced MCNPX model (thin solid line). Measurement results from Tab.3 are depicted as filled symbols those from Tab.2 as open circles. The measured activity for the Cd-covered Au foil is shown as open square, the corresponding simulation as open triangle.

differ by about 10% at this position.

The good agreement between measurements and simulations shows that the spallation target and  $\text{D}_2\text{O}$  moderator perform as expected and that the basic processes of neutron production and moderation are understood in the specific geometry of the PSI UCN source.

## 8. Acknowledgements

We acknowledge the support of Max Ruethi, Michael Meier, the BSQ group, especially Kurt Geissmann and August Kalt, Markus Mähr and the AMI workshops at PSI, Othmar Morath and Pascal Meier of the radiation protection division, Anton Mezger and the PSI accelerator operating crew,

	$a_{\text{tot}}$ ( $kBq/g$ )	$a_{\text{epi}}$ ( $kBq/g$ )	$a_{\text{epi}}/a_{\text{tot}}$
measurement	$152 \pm 10$	$22.8 \pm 1.2$	$0.150 \pm 0.010$
calculation	$175 \pm 10$	$17.3 \pm 2.4$	$0.100 \pm 0.015$

Table 7: Measured (from Tab.2) and simulated specific  $^{198}\text{Au}$  activity from the total,  $a_{\text{tot}}$ , and epithermal,  $a_{\text{epi}}$ , neutron flux, and their ratio (for the position of the Cd covered gold foil) at a height of 117 cm. The  $a_{\text{tot}}$ (measurement) value is interpolated between the two values of Tab.2.

and discussions with Sven Forss. Support by the Swiss National Science Foundation Projects 200020\_137664 and 200020\_149813 is gratefully acknowledged.

## References

- [1] A. Anghel, F. Atchison, B. Blau, B. van den Brandt, M. Daum, R. Dölling, M. Dubs, P.-A. Duperrex, A. Fuchs, D. George, L. Göttl, P. Hautle, G. Heidenreich, F. Heinrich, R. Henneck, S. Heule, T. Hofmann, S. Joray, M. Kasprzak, K. Kirch, A. Knecht, J. Konter, T. Korhonen, M. Kuzniak, B. Lauss, A. Mezger, A. Mtchedlishvili, G. Petzoldt, A. Pichlmaier, D. Reggiani, R. Reiser, U. Rohrer, M. Seidel, H. Spitzer, K. Thomsen, W. Wagner, M. Wohlmuther, G. Zsigmond, J. Züllig, K. Bodek, S. Kistryn, J. Zejma, P. Geltenbort, C. Plonka, S. Grigoriev, The PSI ultra-cold neutron source, Nuclear Instruments and Methods in Physics Research Section A: Accelerators, Spectrometers, Detectors and Associated Equipment 611 (23) (2009) 272 – 275. doi:10.1016/j.nima.2009.07.077.
- [2] B. Lauss, A new facility for fundamental particle physics: The high-intensity ultracold neutron source at the Paul Scherrer Institute, AIP Conference Proceedings 1441 (1) (2012) 576–578. doi:dx.doi.org/10.1063/1.3700622.
- [3] B. Lauss, Startup of the high-intensity ultracold neutron source at the Paul Scherrer Institute, Hyperfine Interactions 211 (2012) 21–25. doi:10.1007/s10751-012-0578-7.
- [4] B. Lauss, Ultracold Neutron Production at the Second Spallation Target

- of the Paul Scherrer Institute, *Physics Procedia* 51 (2014) 98. doi:  
dx.doi.org/10.1016/j.phpro.2013.12.022.
- [5] R. Golub, D. Richardson, S.K. Lamoreaux, *Ultra-Cold Neutrons*, Adam Hilger - Bristol, New York, Philadelphia, 1991.
  - [6] C. Baker, G. Ban, K. Bodek, M. Burghoff, Z. Chowdhuri, M. Daum, M. Fertl, B. Franke, P. Geltenbort, K. Green, M. van der Grinten, E. Gutsmedl, P. Harris, R. Henneck, P. Iaydjiev, S. Ivanov, N. Khomutov, M. Kasprzak, K. Kirch, S. Kistryn, S. Knappe-Grüneberg, A. Knecht, P. Knowles, A. Kozela, B. Lauss, T. Lefort, Y. Lemiere, O. Naviliat-Cuncic, J. Pendlebury, E. Pierre, F. Piegsa, G. Pignol, G. Quémener, S. Roccia, P. Schmidt-Wellenburg, D. Shiers, K. Smith, A. Schnabel, L. Trahms, A. Weis, J. Zejma, J. Zenner, G. Zsigmond, The search for the neutron electric dipole moment at the Paul Scherrer Institute, *Physics Procedia* 17 (2011) 159–167. doi:10.1016/j.phpro.2011.06.032.
  - [7] M. Raidal, A. Schaaf, I. Bigi, M. Mangano, Y. Semertzidis, S. Abel, S. Albino, S. Antusch, E. Arganda, B. Bajc, S. Banerjee, C. Biggio, M. Blanke, W. Bonivento, G. Branco, D. Bryman, A. Buras, L. Calibbi, A. Ceccucci, P. Chankowski, S. Davidson, A. Deandrea, D. DeMille, F. Deppisch, M. Diaz, B. Duling, M. Felcini, W. Fetscher, F. Forti, D. Ghosh, M. Giffels, M. Giorgi, G. Giudice, E. Goudzovskij, T. Han, P. Harris, M. Herrero, J. Hisano, R. Holt, K. Huitu, A. Ibarra, O. Igonkina, A. Ilakovac, J. Imazato, G. Isidori, F. Joaquim, M. Kadastik, Y. Kajiyama, S. King, K. Kirch, M. Kozlov, M. Krawczyk, T. Kress, O. Lebedev, A. Lusiani, E. Ma, G. Marchiori, A. Masiero, I. Masina, G. Moreau, T. Mori, M. Muntel, N. Neri, F. Nesti, C. Onderwater, P. Paradisi, S. Petcov, M. Picariello, V. Porretti, A. Poschenrieder, M. Pospelov, L. Rebane, M. Rebelo, A. Ritz, L. Roberts, A. Romanino, J. Roney, A. Rossi, R. Räckl, G. Senjanovic, N. Serra, T. Shindou, Y. Takanishi, C. Tarantino, A. Teixeira, E. Torrente-Lujan, K. Turzynski, T. Underwood, S. Vempati, O. Vives, Flavor physics of leptons and dipole moments, *The European Physical Journal C* 57 (1-2) (2008) 13–182. doi:10.1140/epjc/s10052-008-0715-2.
  - [8] R. Lamoreaux, S. K. Golub, *The neutron electric dipole moment: Yesterday, today and tomorrow*, *Lepton Dipole Moments. Series: Advanced*

Series on Directions in High Energy Physics, ISBN: 978-981-4271-83-7. WORLD SCIENTIFIC, Edited by B Lee Roberts and William J Marciano, vol. 20, pp. 583-634.

- [9] CERN Council, European Strategy for Particle Physics - Update 2013, s/106 (May 7 2013).
- [10] C. A. Baker, D. D. Doyle, P. Geltenbort, K. Green, M. G. D. van der Grinten, P. G. Harris, P. Iaydjiev, S. N. Ivanov, D. J. R. May, J. M. Pendlebury, J. D. Richardson, D. Shiers, K. F. Smith, Improved experimental limit on the electric dipole moment of the neutron, *Phys. Rev. Lett.* 97 (2006) 131801. doi:10.1103/PhysRevLett.97.131801.
- [11] R.E. Hill, J.M. Anaya, T.J. Bowles, G.L. Greene, G. Hogan, S. Lamoreaux, L. Marek, R. Mortenson, C.L. Morris, A. Saunders, S.J. Seestrom, W. Teasdale, S. Hoedl, C.-Y. Liu, D.A. Smith, A. Young, B.W. Filippone, J. Hua, T. Ito, E. Pasyuk, P. Geltenbort, A. Garcia, B. Fujikawa, S. Baessler, A. Serebrov, Performance of the prototype LANL solid deuterium ultra-cold neutron source, *Nuclear Instruments and Methods in Physics Research Section A: Accelerators, Spectrometers, Detectors and Associated Equipment* 440 (3) (2000) 674 – 681. doi:dx.doi.org/10.1016/S0168-9002(99)01060-8.
- [12] A. Saunders, M. Makela, Y. Bagdasarova, H. O. Back, J. Boissevain, L. J. Broussard, T. J. Bowles, R. Carr, S. A. Currie, B. Filippone, A. Garcia, P. Geltenbort, K. P. Hickerson, R. E. Hill, J. Hoagland, S. Hoedl, A. T. Holley, G. Hogan, T. M. Ito, S. Lamoreaux, C.-Y. Liu, J. Liu, R. R. Mammei, J. Martin, D. Melconian, M. P. Mendenhall, C. L. Morris, R. N. Mortensen, R. W. Pattie, M. Pitt, B. Plaster, J. Ramsey, R. Rios, A. Sallaska, S. J. Seestrom, E. I. Sharapov, S. Sjue, W. E. Sondheim, W. Teasdale, A. R. Young, B. VornDick, R. B. Vogelaar, Z. Wang, Y. Xu, Performance of the Los Alamos National Laboratory spallation-driven solid-deuterium ultra-cold neutron source, *Review of Scientific Instruments* 84 (1). doi:dx.doi.org/10.1063/1.4770063.
- [13] D. Pelowitz (Ed.), *MCNPX<sup>TM</sup> User's Manual*. Version 2.7.0, no. LA-CP-11-00438, LANL, 2011.
- [14] M. Seidel, S. Adam, A. Adelmann, C. Baumgarten, Y.J. Bi, R. Doelling, H. Fitze, A. Fuchs, M. Humbel, J. Grillenberger, D. Kiselev, A. Mezger,

- D. Reggiani, M. Schneider, J.J. Yang, H. Zhang, T.J. Zhang, Production of a 1.3 MW proton beam at PSI, Proceedings of IPAC10, Kyoto, Japan TUYRA03 (2010) 1309.
- [15] J. Grillenberger, M. Humbel, A. Mezger, M. Seidel, W. Tron, Status and further development of the PSI high intensity proton facility, Proceedings of Cyclotrons2013, Vancouver, BC, Canada MOPPT004 (2013) 1.
  - [16] M. Wohlmuther, G. Heidenreich, The spallation target of the ultra-cold neutron source UCN at PSI, Nuclear Instruments and Methods in Physics Research Section A: Accelerators, Spectrometers, Detectors and Associated Equipment 564 (1) (2006) 51–56.
  - [17] K. Kirch, B. Lauss, P. Schmidt-Wellenburg, G. Zsigmond, Ultracold neutrons — physics and production, Nucl. Phys. News 20:1 (2010) 17–23.
  - [18] D. Anicic, M. Daum, G. Dzieglewski, D. George, M. Horvat, G. Janser, F. Jenni, I. Jirousek, K. Kirch, T. Korhonen, R. Kaenzi, A. Mezger, U. Rohrer, L. Tanner, A fast kicker magnet for the PSI 600 MeV proton beam to the PSI ultra-cold neutron source, Nuclear Instruments and Methods in Physics Research Section A: Accelerators, Spectrometers, Detectors and Associated Equipment 541 (3) (2005) 598–609.
  - [19] D. Reggiani, First proton beam pulses to the UCN target, Technical Report TM-85-10-04, Paul Scherrer Institut (2010, unpublished).
  - [20] F. Atchison, Calculated values for heating, particle fluxes and activation in components of the UCN source, SUNS, TM-14-02-02, Technical report, Paul Scherrer Institut (2002, unpublished).
  - [21] W. Wagner, M. Wohlmuther, U. Stuhr, V. Davydov, J. Repper, S. Van Petegem, U. Filges, B. Blau, B. Lauss, L. Goeltl, M. Hildebrandt, K. Thomsen, B. Hammer, J. Neuhausen, D. Schumann, SINQ and UCN two high-power spallation sources operating at PSI, in: Proceedings of the International Collaboration on Advanced Neutron Sources, ' ICANS XX ' March 4 - 9, 2012 Bariloche, Ro Negro, Argentina, 2012.



- [22] V. Talanov, On the numerical estimation of the primary neutron yield from the spallation target of the UCN source, Technical Report TM-85-13-04, Paul Scherrer Institut (2013, unpublished).
- [23] G.A. Bartholomew, P.R. Tunncliffe, The AECL study for an Intense Neutron-Generator (Technical Details) (July 1966).
- [24] Evaluated Nuclear Structure Data File ( ENSDF), National Nuclear Data Center, Brookhaven National Laboratory, 2014.  
URL [www.nndc.bnl.gov/ensdf/](http://www.nndc.bnl.gov/ensdf/)
- [25] V. Talanov, Numerical simulation of the gold foil activation for the irradiation experiment at the UCN source, Technical Report TM-85-13-14, Paul Scherrer Institut (2013, unpublished).
- [26] R. Forrest, FISPACT-2007: User manual, Technical Report UKAEA FUS 534, EURATOM / UKAEA (2007).
- [27] F.X. Gallmeier, W.L. Wilson, M. Wohlmuther, B. Micklich, E.B. Iverson, E. Pitcher, W. Lu, H.R. Trellue, Ch. Kelsey, G. Muhrer, I.I. Popova, P.D. Ferguson, An environment using nuclear inventory codes in combination with the radiation transport code MCNPX for accelerator activation problems, in: Proceedings of ACCAPP'07, Pocatello, Idaho, 2007, pp. 207–211.